J Supercond Nov Magn (2011) 24:2137–2144
DOI 10.1007/s10948-011-1168-7

ORIGINAL PAPER

Structural, Electrical and Dielectric Properties of Co–Mn Spinel Nanoferrites Prepared by Co-precipitation Technique

Tasawar Javed · Asghari Maqsood · Akhlaq Ahmed Malik

Received: 2 March 2011 / Accepted: 29 March 2011 / Published online: 21 April 2011

Abstract Cobalt manganese nanoceramics with nominal composition $Co_{1-x}Mn_xFe_2O_4$ ($x = 0.00, 0.15, 0.30, 0.45, 0.60, 0.75$) were synthesized by a chemical coprecipitation technique. The X-ray diffraction patterns revealed the cubic spinel structure. The average crystallite size from the Sherrer formula was in the range of 28 nm–56 nm. The lattice parameter increased with a concentration of manganese. Scanning electron microscopy (SEM) was used for microstructural study. The electrical properties such as electrical resistivity (ρ), drift mobility (μ_d), and activation energy (ΔE) were measured using a two-probe apparatus in the temperature range 323–573 K. The electrical resistivity decreased with temperature and manganese concentration. The dielectric constant (ε'), loss factor or imaginary loss (ε'') and dielectric tangent loss ($\tan\delta$) were measured at room temperature using a LCR meter in the frequency range 100 Hz to 5 MHz. All the dielectric parameters decreased with increasing frequency. The AC electrical conductivity (σ_{ac}) was calculated from the dielectric measurements. It increases with increase of frequency and manganese concentration. The increase in electrical conductivity may be attributed to the formation of Co^{+3} and Mn^{+3} from Co^{+2} and Mn^{+3}, respectively, at both A and B sites.

T. Javed (✉) · A. Maqsood
Thermal Transport laboratory, School of Chemical and Materials Engineering (SCME), National University of Sciences and Technology (NUST) H-12, Islamabad, Pakistan
e-mail: sunotasawar@hotmail.com

A. Maqsood
e-mail: tpl.qau@usa.ne

T. Javed · A.A. Malik
Department of Metallurgical and Materials Engineering, University of Engineering and Technology (UET), Lahore, Pakistan

Keywords AC conductivity · Coprecipitation · DC resistivity · Dielectric constant · Nanoceramics

1 Introduction

Synthesis of nanoparticles with controlled size has always been a challenge for the scientists and engineers. Many techniques, like sol-gel [1], sonochemical [2], micro emulsion [3], combustion [4], hydrothermal [5], etc. have been employed. The chemical coprecipitation method is economical and easy to commercialize. Soft magnetic ferrites are technologically very important industrial materials. These have good chemical inertness, high mechanical strength, excellent corrosion resistance, high resistivity, high Curie's temperature, and good magnetooptic properties. Nanoferrites have become of considerable attention during the last few years. The quantum confinement phenomenon becomes well pronounced in these materials. Co–Mn nanoferrites are very important because they present better magnetic and dielectric properties. They are also good candidate materials for applications like negative temperature coefficient thermistor [6], inductor cores in TV circuits, generators, rotors, stators, microwave devices, and data storage devices.

2 Experimental Procedure

The nanoferrite powders with the composition $Co_{1-x}Mn_xFe_2O_4$ (with $0.0 \leq x \leq 0.75$) were prepared by the chemical coprecipitation method. The chemical used were: $Fe(NO_3)_2 \cdot 9H_2O$, $Co(NO_3)_2 \cdot 6H_2O$, and $Mn(NO_3)_2 \cdot 4H_2O$. All the chemicals were of high purity and analytical grade. The precipitating agent was NaOH. The aqueous solutions of the chemicals $Fe(NO_3)_2 \cdot 9H_2O$, $Mn(NO_3)_2 \cdot 4H_2O$, and

$Co(NO_3)_2{\cdot}6H_2O$ in their stoichiometry (100 ml of 0.2 molar $Fe(NO_3)_2{\cdot}9H_2O$, 100 ml of 0.015 $Mn(NO_3)_2{\cdot}4H_2O$, and 100 ml of 0.085 molar $Co(NO_3)_2{\cdot}6H_2O$ in case of $Co_{0.85}Mn_{0.15}Fe_2O_4$ and similarly for other values of x) were prepared in de-ionized water and heated to 70 °C with continuous stirring. The aqueous solution of the coprecipitating agent (200 ml of 1.5 molar NaOH) was made separately in deionized water and heated to 90 °C with constant stirring. The metal salts solutions were then mixed and stirred for 2 hours to obtain a homogeneous mixture. The NaOH solution was added to the salt solutions in a continuous stream with constant stirring of 300 r.p.m. The reaction temperature was kept at 90 °C and PH was maintained at 12 to ensure the complete precipitation. After 40 min, the heating was stopped and stirring continued for 2 hours. The samples were then washed 5–6 times with de-ionized water and dried in an electric oven at 100 °C for overnight. The samples were calcined at 850 °C for 8 hours in a box furnace and allowed to cool in the furnace. The powder samples were then grinded in a cleaned agate mortar and pestle for 1 hour. Finally, the powders were formed into pellets shape by using hydraulic press, applying a constant pressure of 68 KN for 3 minutes in each of the compositions and the pelletized samples were sintered at 450 °C in the same furnace.

3 Results and Discussion

3.1 XRD Analysis

X-ray diffraction (XRD) analysis confirmed the single phase cubic spinel structure of the synthesized samples. XRD patterns of all the samples are shown in Fig. 1. The (311) peak was observed to be the most intense peak in all the XRD patterns. The average crystallite size was determined using Sherrer's formula [7]. The crystallite size [8] decreased with increasing concentration of manganese. The crystallite size was in the range 28–56 nm. The lattice parameter (a) was also calculated from the results. It increased with increasing manganese substitution. The lattice parameter as measured was in the range 8.3783–8.4474 Å and is listed in Table 1. The increase in lattice constant was due to the larger ionic radius of Mn^{+2} ions (0.80 Å) as compared to Co^{2+} (0.72 Å). A partial substitution of cobalt with manganese increases the unit cell dimensions, and ultimately unit cell parameter and volume increases.

3.1.1 Measured Density

The measured density (ρ_m or D_m) was determined using the following standard formula [9]:

$$D_m = \frac{m}{\pi r^2 h} \tag{1}$$

where m is the mass, r is the radius, and h is the thickness of the sample.

The variation of measured density and porosity with manganese concentration is shown in Fig. 2. The measured density was found to increase from 2.760 to 3.315 g/cm^3. The increase in density may be attributed to diffusion of Mn ions to the lattice and the increasing reactivity of the fine grains of the materials which subsequently coalesce to form bigger grains. Resultantly, there is a reduction in the number of pores.

3.1.2 X-ray Density

X-ray density was measured using the formula [9].

$$D_x = \frac{8M}{Na^3} \tag{2}$$

where "M" is the molecular weight of the samples, "N" is the Avogadro's number and "a" is the lattice constant.

The X-ray density of all the samples is listed in Table 1. The X-ray density of all the samples decreased with manganese content and was in the range 5.300 to 5.103 g/cm^3. This was due to the fact that atomic weight of the manganese is less than that of cobalt. It was observed that X-ray density of each sample is greater than its corresponding measured density. This was due to the pores present in the prepared materials.

3.1.3 Porosity

The porosity for all the samples was measured using the formula [8].

$$P = 1 - \frac{D_m}{D_x} \tag{3}$$

where D_m, D_x are the measured and X-ray densities, respectively.

The value of porosity decreases with manganese concentration. It varies from 0.478 to 0.450. The values of porosity for all the compositions are listed in Table 1. The decrease in the porosity was expected as described above. As the manganese content increases, the number of pores is reduced due to increase of grain size. Smaller grains coalesce to form larger grains and resultantly grain to grain contact area increases and porosity decreases.

3.1.4 Surface Area

The specific surface area (m^2/g) of ferrites was calculated from the relation [9].

$$S = \frac{6000}{t D_m} \tag{4}$$

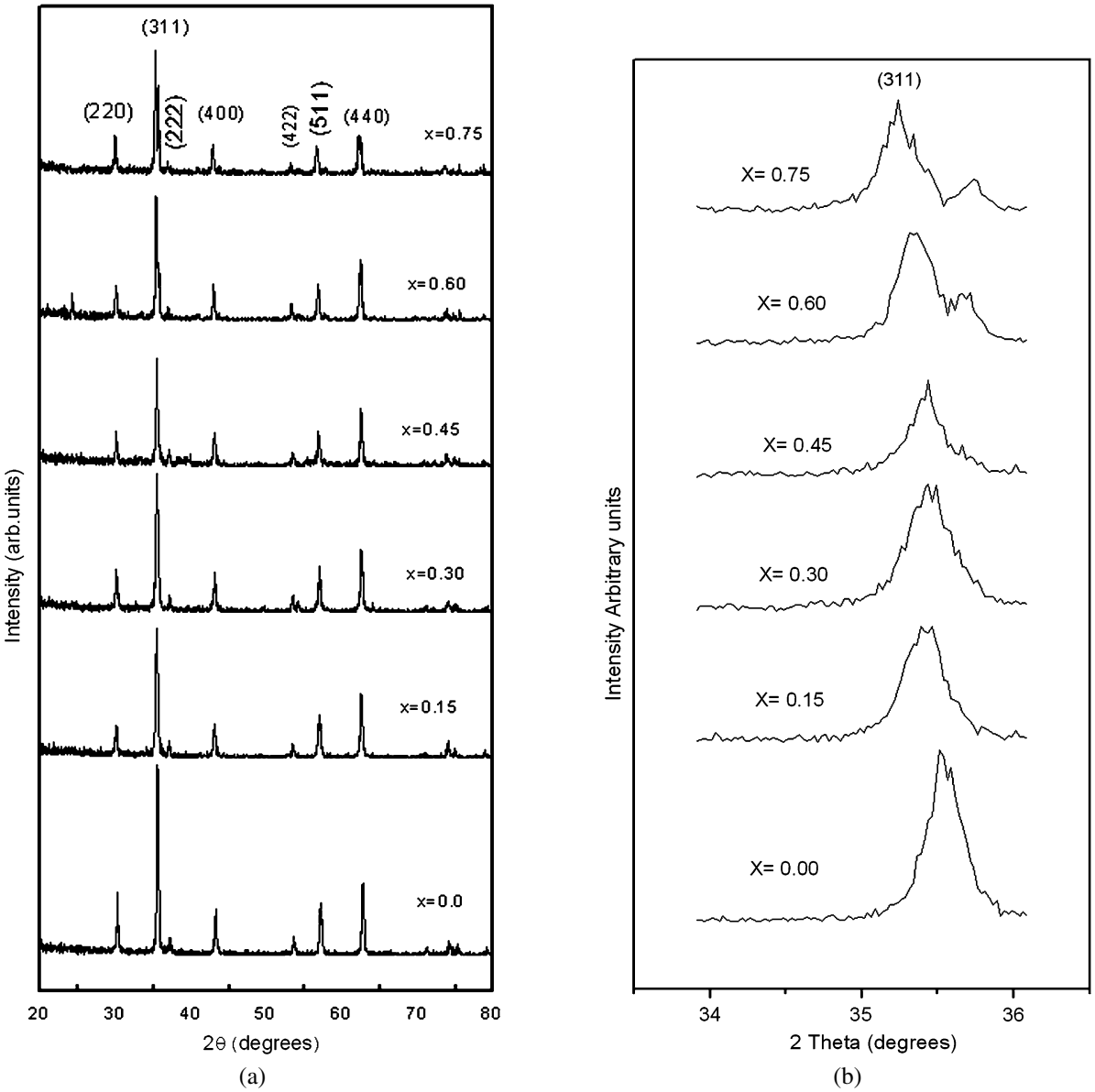

Fig. 1 **a** Indexed XRD patterns of $Co_{1-x}Mn_xFe_2O_4$ (peak at $2\theta = 24$ degrees in $x = 0.60$ is the impurity Fe_2O_3). **b** Enlarged (311) XRD peaks for $Co_{1-x}Mn_xFe_2O_4$

where 't' is the diameter of the particles in nm and D_m the measured density in g/cm^3.

The surface area increases with increase in manganese and is listed in Table 1. The inverse relationship between the surface area and diameter of the particles is confirmed by results.

3.2 DC Electrical Resistivity

DC electrical resistivity of all the samples was measures using two probes apparatus [10] in the temperature range of 300 K to 573 K. The DC resistivity of all the samples decreased with increasing temperature ensuring the semiconducting nature of the nano-ceramics. The DC resistivity measured at 413 K was in the range 0.42×10^5 to 10.02×10^5 Ω-cm with $0.0 \leq x \leq 0.75$. The DC resistivity decreases with increase of manganese from 0.0 to 0.75. The variation of resistivity with inverse of temperature is shown in Fig. 3. The values for each composition are listed in Table 1. The decrease in resistivity may be attributed to distribution of cations at A and B sites and the fact that Mn occupies A sites favorably. According to Kue Hong Kim et al. [11] $Co_{1-x}Mn_xFe_2O_4$ ceramics show n-type conduction [12], as was explained by Seebeck coefficient measurements [13], which is attributed to the formation Co^{+3} and Mn^{+3} ions from the doubly charged cations. So possibility of charge transfers between valence states of +2 and +3 of

Table 1 Average crystallite size (t), lattice constant (a), lattice volume (V), X-ray density (D_x), measured density (D_m), porosity (P), specific surface area (S), DC electrical resistivity (ρ), activation energy (ΔE), correlation coefficient (R), drift mobility (μ_d), DC conductivity (σ_{dc}), AC conductivity (σ_{ac}), dielectric constant (ε') and tangent loss ($\tan\delta$) of $Co_{1-x}Mn_xFe_2O_4$ ($0.0 \le x \le 0.75$) ferrite nanoparticles

Parameter	Mn concentration					
	$x = 0.0$	$x = 0.15$	$x = 0.30$	$x = 0.45$	$x = 0.60$	$x = 0.75$
t (311) (nm) $\pm$ 2	56	28	42	40	39	34
a (Å)	8.3783	8.3974	8.3977	8.4055	8.4235	8.4474
V (Å)^3	588	592	592	594	598	603
D_m (g/cm^3) $\pm$ 0.001	2.766	2.771	2.785	2.823	2.951	3.315
D_x (g/cm^3) $\pm$ 0.001	5.300	5.250	5.238	5.207	5.159	5.103
P (fraction) $\pm$ 0.001	0.478	0.472	0.468	0.458	0.428	0.350
S (m^2/g)	39	77	51	51	42	53
ρ (Ω-cm) at 413 K $\times 10^5$	10.02	4.75	2.35	1.17	0.65	0.42
μ_d (cm^2 V^{-1} s^{-1}) $\times 10^{-10}$	4.3	8.9	18.0	38.0	56.0	97.0
ΔE (eV) $\pm$ 0.001	0.551	0.498	0.458	0.420	0.412	0.367
R	0.99	0.99	0.99	0.99	0.99	0.99
σ_{dc} (S cm^{-1}) $\times 10^{-5}$ 413 K	0.144	0.296	0.550	1.090	2.020	3.020
σ_{ac} (S cm^{-1})100 KHz $\times 10^{-4}$	0.38	1.44	1.76	1.87	1.91	1.99
σ_{ac} (S cm^{-1}) 2 MHz $\times 10^{-4}$	2.10	4.41	8.61	8.64	12.00	12.30
ε' at 100 Hz $\times 10^3$	0.317	5.21	11.08	15.04	24.67	32.51
ε' at 5 MHz	12.4	13.8	14.5	14.5	15.8	16.8
$\tan\delta$ at 100 Hz	1.99	4.04	5.55	6.37	6.99	8.34
$\tan\delta$ at 5 MHz	0.079	0.101	0.110	0.167	0.179	0.246

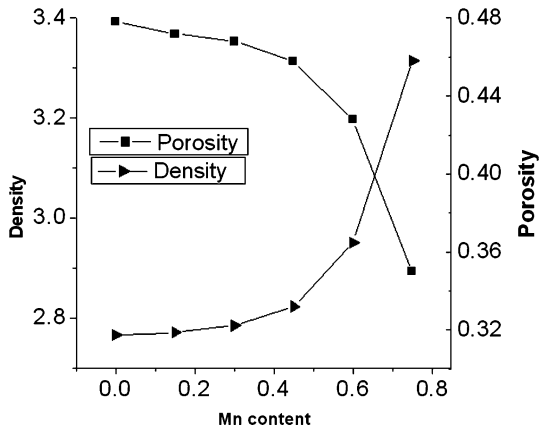

Fig. 2 Variation of measured density (g/cm^3) and porosity with Mn content in $Co_{1-x}Mn_xFe_2O_4$

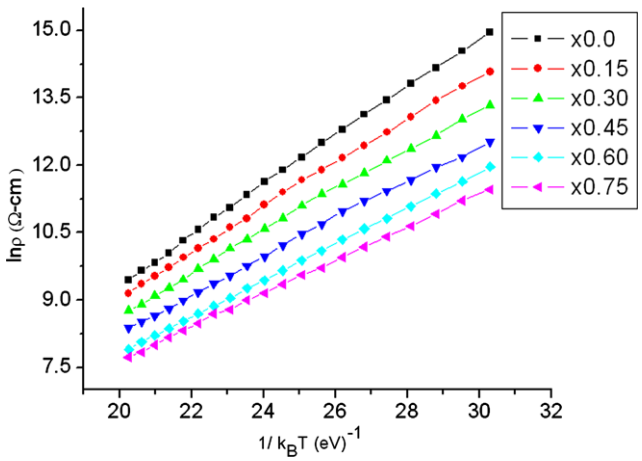

Fig. 3 Variation of DC resistivity ($\ln\rho$) with inverse temperature ($1/k_BT$) for $Co_{1-x}Mn_xFe_2O_4$

the cations at A and B sites may contribute to the decrease in resistivity. If the +2 ions at A sites do not contribute to the decrease in resistivity then it may be attributed to the incorporation of oxygen non stoichiometry [14] which produces additional +2 ions at B site. The decrease in resistivity due to the substitution of manganese is due to the fact that Mn ions go preferentially to the A sites and Co ions to A and B sites. When the concentration of Mn increases at A sites, the concentration of Co ions at B sites decreases. This favors the migration of some of the Fe ions from A to B sites.

As a result of this, the hopping between Fe^{+2} and Fe^{+3} (which is responsible for the conduction in ferrites) increases and resistivity decreases. In a true sense, resistivity is the result of combined factors like microstructure homogeneity, crystal structure grain size, and imperfections in the ferrites.

The activation energy [15], which is the energy responsible for hopping between +2 and +3 states of cations, and hence the mobility, was calculated for $Co_{1-x}Mn_xFe_2O_4$ $0.0 \le x \le 0.75$. The activation energy was calculated from the slopes of the linear graphs of resistivity and inverse temperature using the well-known Arrhenius equation [16].

$$\rho = \rho_0 \exp\left(\frac{\Delta E}{k_B T}\right) \tag{5}$$

where k_B is the Boltzmann constant, T is temperature expressed in Kelvin, and ΔE is the activation energy.

The activation energy values are listed in Table 1. The calculated activation energy values were in the range 0.551 to 0.361 eV for $0.0 \leq x \leq 0.75$. The activation energy values decreased with an increase of manganese substitution. It is fact that conduction in ferrites is due to the hopping of the electron between Fe^{+2} and Fe^{+3} at octahedral sites and the activation energy is responsible for the hopping. So, activation energy determines the conductivity and resistivity. The change in Arrhenius slopes may be attributed to the change of the conduction mechanism in the ferrite samples. The Fe^{+2}–Fe^{+3} hopping are responsible for the conduction at low temperatures while the conduction at high temperature is due to the polaron hopping. A similar kind of behavior has been reported by Vijaya Puri et al. [17].

Drift mobility (μ_d) [18] for the synthesized compositions $Co_{1-x}Mn_xFe_2O_4$ $0.0 \leq x \leq 0.75$ was calculated using the relation.

$$\mu_d = \frac{1}{ne\rho} \tag{6}$$

where e is the charge of electron, ρ is the electrical resistivity and n is the concentration of charge carrier and can be calculated from the famous equation [19].

$$n = \frac{N D_m P_{Fe}}{M} \tag{7}$$

where N, D_m, and M have already been defined above and P_{Fe} is the number of iron atoms in the chemical formula of the respective ferrites.

The drift mobility increases with increasing manganese contents and is shown in Fig. 4. The drift mobility was found in the range 4.3×10^{-10} to 97×10^{-10} $cm^2\,V^{-1}\,s^{-1}$ with $0.0 \leq x \leq 0.75$. It has been observed that there exists an inverse relationship between resistivity and drift mobility.

DC conductivity was also calculated from the resistivity measurements. The DC conductivity values varied in the range 0.144 to 3.02×10^{-5} S/cm at 413 K with $0.0 \leq x \leq 0.75$. The reasons for the increase in DC conductivity have been explained above. The graphs for DC conductivity are shown in Fig. 5.

3.3 Dielectric Properties

The dielectric constant (ε') for the compositions $Co_{1-x}Mn_xFe_2O_4$ $0 \leq x \leq 0.75$ was calculated by the relation [20].

$$\varepsilon' = \frac{Cd}{\varepsilon_0 A} \tag{8}$$

where C is capacitance in Farad, d is the thickness of the pellets in m, A is the cross-sectional area of flat surface of the pellets in m^2, and ε_0 is the permittivity of free space.

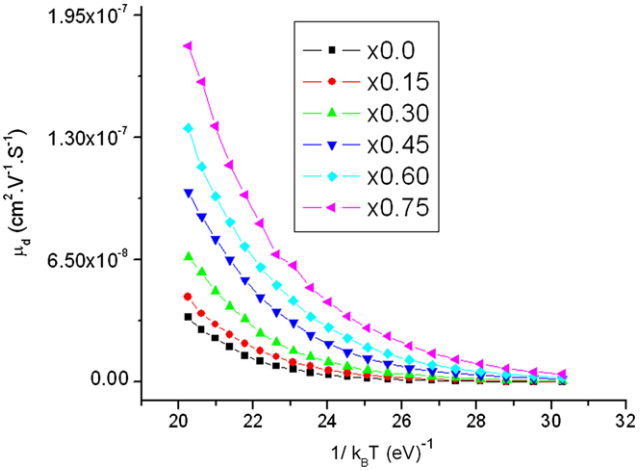

Fig. 4 Temperature dependence of drift mobility (μ_d) of $Co_{1-x}Mn_xFe_2O_4$

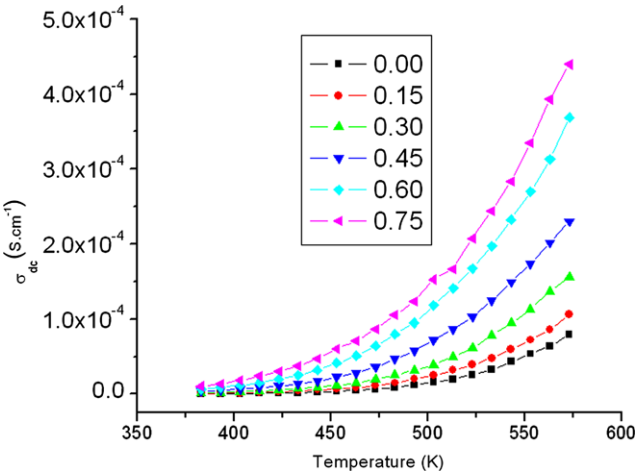

Fig. 5 DC conductivity (σ_{dc}) as a function of temperature for $Co_{1-x}Mn_xFe_2O_4$

The dielectric constants measurements were done in the range 100 Hz to 5 MHz using WAYNE KERR LCR METER (6500B). The values for dielectric constant at different frequencies are listed in Table 1. The plots of dielectric constant against frequency are depicted in Fig. 6. Dielectric constant increases with increasing concentration of manganese and decreases with increasing frequency. This dependence upon frequency is because of the interfacial polarization as predicted by Maxwell–Wagner [21]. According to the Maxwell–Wagner model, the dielectric structure of a ferrite material is assumed to be made up of two layers; the first layer being a conductive layer that consists of large ferrite grains and the other being the grain boundaries that are poor conductors. According to Rabinkin and Novikova [22], the polarization in ferrites is through a mechanism similar to the conduction process. By the electron exchange between Fe^{+2} and Fe^{+3}, the local displacement of electrons in the direction of the applied field occurs and these elec-

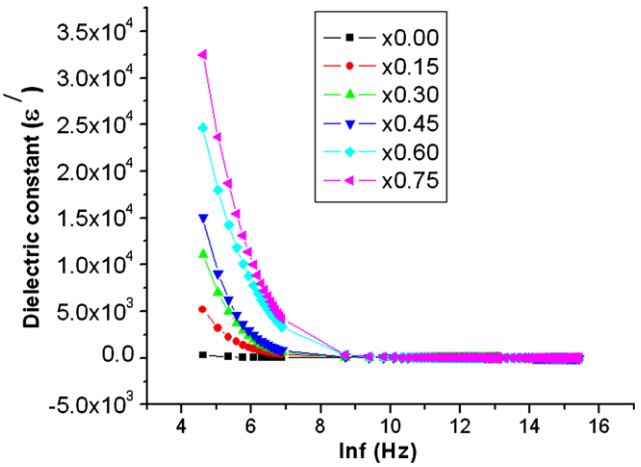

Fig. 6 Frequency dependence of dielectric constant (ε') for $Co_{1-x}Mn_xFe_2O_4$

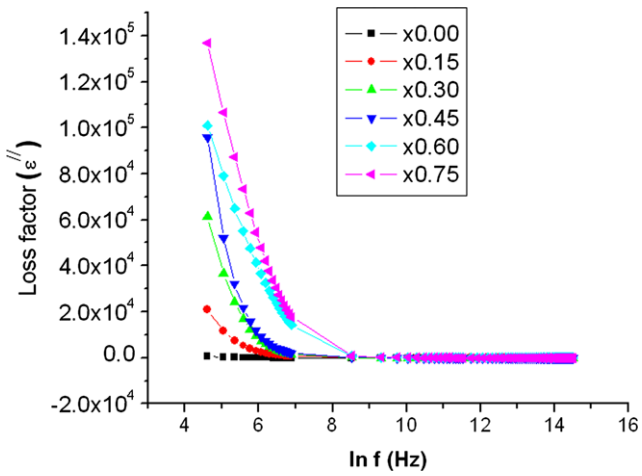

Fig. 7 Dielectric loss (ε'') as a function of frequency for $Co_{1-x}Mn_xFe_2O_4$

trons determine the polarization. The large value of dielectric constant (ε') at lower frequency is due to the predominance of species like Fe^{2+} ions, interfacial dislocations pile ups, oxygen vacancies, grain boundary defects, etc., while the decrease in (ε') with frequency is natural because of the fact that any species contributing to polarizability is found to show lagging behind the applied field at higher and higher frequencies. The decrease in dielectric constant with an increase in frequency is due to the fact that the polarization decreases with increasing frequency and then reaches a constant value. By increasing the frequency beyond a certain frequency limit, the electron hopping cannot follow the electric field fluctuations; this causes a decrease in the dielectric constant. According to the Koop's model, the dielectric constant at low frequency comes from the grain boundaries which have a high dielectric constant due high resistivity at the grain boundary region. The dielectric constant at high frequency comes from the grains which have a small dielectric constant values due to low resistivity. It was concluded that the electron exchange between Fe^{+2} and Fe^{+3} ions results in the direction of an electric field, which is responsible for electrical polarization in ferrites. For the Co–Mn ferrites, the incorporation of Mn^{+2} in the octahedral (B) site may decrease the concentration of Fe^{+3}–Fe^{+2} ion pairs. The magnitude of exchange depends on the concentration of Fe^{+3}–Fe^{+2} ion pairs present at the B site. The higher value of dielectric constant at low frequency is due to voids, dislocations and other defects.

Dielectric loss factor (ε'') was also calculated from dielectric tangent loss ($\tan\delta$) using the relation [23]

$$\tan\delta = D = \frac{\varepsilon''}{\varepsilon'} \tag{9}$$

where ε'' is the imaginary part of the dielectric constant and is a measure of the absorption of energy by the dielectric

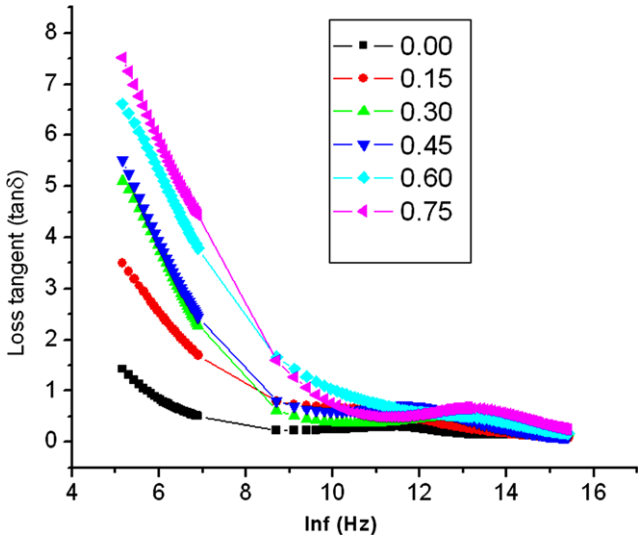

Fig. 8 Dielectric loss tangent ($\tan\delta$) as unction of frequency for $Co_{1-x}Mn_xFe_2O_4$

from the alternating field, δ is the loss angle and ε' is the real part of the dielectric constant.

The dielectric loss (ε'') or imaginary part of the dielectric loss and tangent loss ($\tan\delta$) decrease with increase of frequency and then become constant at higher frequencies. The values or both the factors at different frequencies are tabulated in Table 1. Figures 7 and 8 show the plots for imaginary loss and tangent loss, respectively. Both the factors decrease continuously at low frequency with increasing Mn^{+2} concentrations. The decrease in dielectric loss (ε'') with increasing frequency is attributed to the decrease in the polarization of the sample because the dipoles cannot follow up the field variation. The dielectric tangent loss ($\tan\delta$) also decreases with increase in frequency and decrease in manganese concentration. The decrease in loss tangent with frequency may be attributed to the Maxwell–Wagner polarization and con-

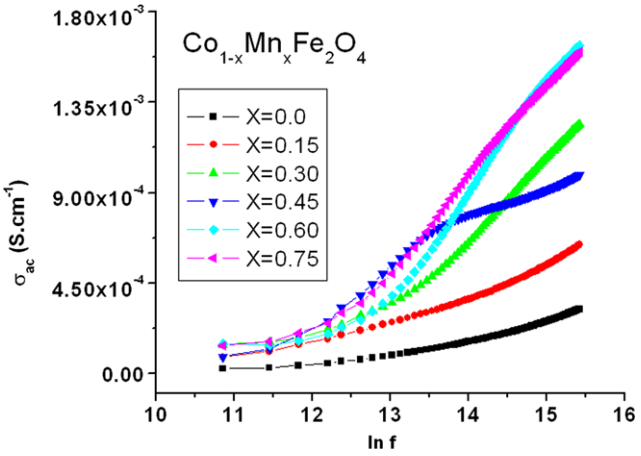

Fig. 9 AC conductivity as function of frequency for $Co_{1-x}Mn_xFe_2O_4$ at room temperature

duction mechanism in ferrites. The decrease in loss tangent with Mn may be attributed to the increase in structural inhomogeneity due to incorporation of the Mn into the lattice.

The AC conductivity (σ_{ac}) was also calculated by using the relation $\sigma \alpha c = 2\pi f \varepsilon' \varepsilon_0 \tan\delta$ where f is frequency and all other factors have been described above. The values of AC conductivity are listed in Table 1. Figure 9 shows that AC conductivity increases with increase in frequency and manganese contents. Frequency dependence of AC conductivity may be attributed to the structural parameters in the ferrites like grain boundaries, dislocations, density, etc. AC conductivity behavior is in accordance with the earlier studies [24, 25].

3.4 Scanning Electron Microscopy (SEM)

The average grain size was determined using the relation [26].

$$G_a = \frac{1.5L}{MN} \tag{10}$$

where L is the total test line length; M the magnification; N is the total number of intercepts. Scanning electron micrographs for the two samples $x = 0.0$ and $x = 0.75$ are shown in Fig. 10. The estimated average grain size for the two end members was 0.15 μm and 0.40 μm, respectively. It has been observed that the grain size increases with increase of manganese concentration. The increase in grain size may be attributed to the enhanced solid state solubility of manganese in the reaction at higher concentrations.

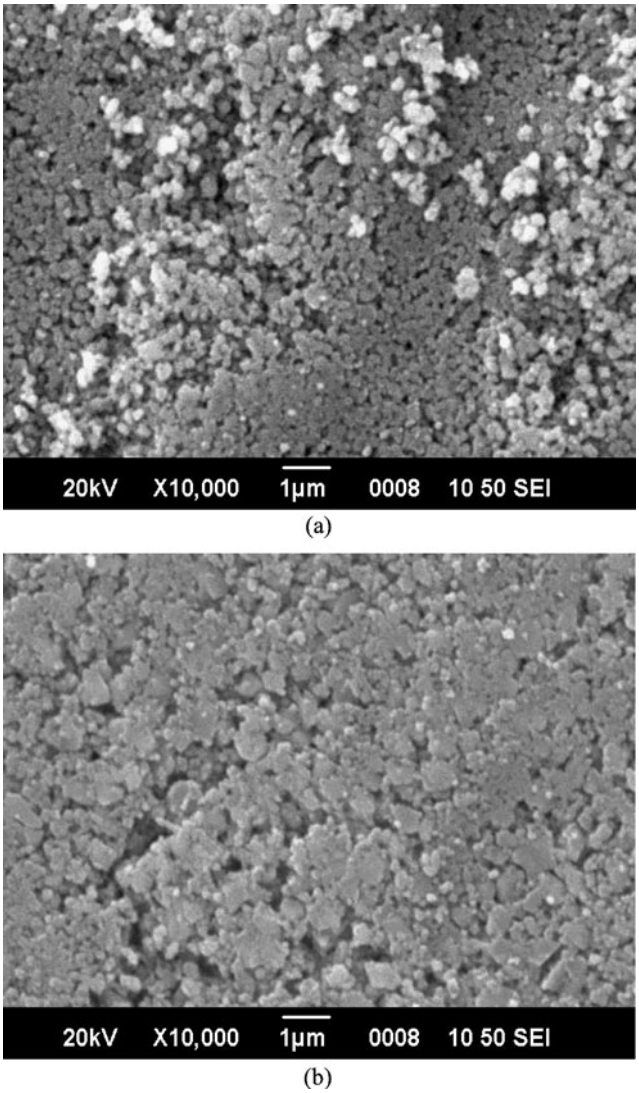

Fig. 10 SEM images for $Co_{1-x}Mn_xFe_2O_4$ **a** $x = 0.0$, **b** $x = 0.75$

4 Conclusions

Coprecipitation comes out to be a simple and economical method for the preparation of nanoferrites with controlled diameter. Substitution of manganese in $Co_{1-x}Mn_xFe_2O_4$ $0.0 \leq x \leq 0.75$ produces useful structural, electrical, and dielectric changes. Lattice parameter and measured density increase linearly. Crystallite size and porosity fraction decrease with Mn concentration. DC electrical resistivity and activation energy decrease; drift mobility and DC conductivity decrease with Mn. Resistivity also decreases at higher temperatures. The dielectric constant decreases appreciably at higher frequencies and increases with Mn. The high value of the dielectric constant might be very useful in capacitors used in the electronic devices like memory cards, computers, and many other components. Co–Mn ceramics may also prove very useful materials for microwave applications and other small scale electronics (microelectronics) and may be good candidate materials for the miniaturization of modern electronic components. Electromagnetic properties are also enhanced to a great extent by substitution of manganese.

Co–Mn may also prove useful for negative temperature coefficient thermistors. The quality factor is also improved by the substitution of Mn.

Acknowledgements The authors are greatly thankful to Ms. Humaira Anwar (Research scholar) and Ms. Irum Pervaiz (Ph.D. student) for their support in resistivity measurements. They are also thankful to Mr. Kishwar Khan, Mr. Aftab Akram, and Ahmad Faraz for useful discussions and moral support. The financial support of PSF through Project No. 147 is also acknowledged.

References

1. Shobana, M.K., Sankar, S.: J. Magn. Magn. Mater. **321**, 599–601 (2009)
2. Lv, W.-Z., Liu, B., Luo, Z.-K., Ren, X.-Z., Zhang, P.-X.: J. Magn. Magn. Mater. **321**, 599–601 (2009)
3. Wang, J., Chong, P.F., Ng, S.C., Gan, L.M.: Mater. Lett. **30**, 217–221 (1997)
4. Arjunwadkar, P.R., Patil, R.R., Kulkarni, D.K.: J. Alloys Compd. **463**, 403–407 (2008)
5. Huo, J., Wei, M.: Mater. Lett. **63**, 1183–1184 (2009)
6. Fawzi, A.S., Sheikh, A.D., Mathe, V.L.: J. Alloys Compd. **502**, 231–237 (2010)
7. Mathur, P., Thakur, A., Singh, M.: J. Magn. Magn. Mater. **320**, 1364 (2008)
8. Gul, I.H., Abbasi, A.Z., Amin, F., Anis-ur-Rehman, M., Maqsood, A.: J. Magn. Magn. Mater. **311**, 494–499 (2007)
9. Gul, I.H., Amin, F., Abbasi, A.Z., Anis-ur-Rehman, M., Maqsood, A.: Scr. Mater. **56**, 497–500 (2007)
10. Naeem, M., Shah, N.A., Gul, I.H., Maqsood, A.: J. Alloys Compd. **487**, 739–743 (2009)
11. Lee, D.H., Kim, H.S., Yo, C.H., Ahn, K., Kim, K.H.: Mater. Chem. Phys. **57**, 169–172 (1998)
12. Smit, J., Wijin, H.P.J.: Ferrites. Wiley, New York (1959)
13. Lee, D.H., Ryu, K.H., Kim, Y.Y., Kim, K.H.: Mater. Chem. Phys. **38**, 377 (1994)
14. Gallaso, F.S.: Structure and Properties of Inorganic Solids. Pergamon Press, Oxford (1970)
15. Gul, I.H., Ahmed, W., Maqsood, A.: J. Magn. Magn. Mater. **320**, 270–275 (2008)
16. Gul, I.H., Maqsood, A.: J. Alloys Compd. **465**, 227–231 (2008)
17. Jadhav, R.N., Puri, V.: J. Alloys Compd. **507**, 151–156 (2010)
18. Berchmans, L.J.: J. Magn. Magn. Mater. **279**, 103 (2004)
19. Mott, N.F., Davis, E.A.: Electronic Proc. in Non-Cryst. Mat. Clarendon Press, Oxford (1979)
20. Brockman, F.G., Dowling, P.H., Steneck, W.G.: Phys. Rev. **75**, 1440 (1949)
21. Wagner, K.W.: Ann. Phys. **40**, 817 (1913)
22. Rabinkin, I.T., Novikova, Z.I.: Ferrites. Izv. Acad. Nauk USSR, Minsk (1960), pp. 146
23. Maqsood, A., Khan, K.: J. Alloys Compd. **509**, 3393–3397 (2011)
24. Mahalakshmi, S., Srinivasa, K.: J. Alloys Compd. **457**, 522–525 (2008)
25. Maqsood, A., Khan, K., Anis-ur-Rehman, M., Malik, M.A.: J. Supercond. Nov. Magn. (2010). doi:10.1007/s10948-010-0956-9
26. Wurst, J.C., Nelson, J.A.: J. Am. Ceram. Soc. **55**, 109 (1972)